Variability of the Lagrangian turbulent diffusivity in the lower stratosphere

B. Legras, I. Pisso, Gwenaël Berthet, Franck Lefèvre

Atmos. Chem. Phys. Discuss., 4, 8285–8325, 2004
www.atmos-chem-phys.org/acpd/4/8285/
SRef-ID: 1680-7375/acpd/2004-4-8285
European Geosciences Union

Atmospheric Chemistry and Physics Discussions

Variability of the Lagrangian turbulent diffusivity in the lower stratosphere

B. Legras[1], **I. Pisso**[1], **G. Berthet**[2], **and F. Lefèvre**[2]

[1]Laboratoire de Météorologie Dynamique, UMR8539, Paris, France
[2]Service d'Aéronomie, UMR7620, Paris, France

Received: 28 October 2004 – Accepted: 9 November 2004 – Published: 15 December 2004

Correspondence to: B. Legras (legras@lmd.ens.fr)

Abstract

Ozone and nitrous oxide are measured at high spatial and temporal resolution by instruments flying on the ER-2 NASA research aircraft. Comparing the airborne transects to reconstructions by ensemble of diffusive backward trajectories allows to estimate the average vertical Lagrangian turbulent diffusion experienced by the air parcels. The resulting estimates show large Lagrangian diffusion of the order of $0.1\,m^2\,s^{-1}$ outside the polar vortex in the surf zone and smaller values of the order of $0.01\,m^2\,s^{-1}$ inside. Locally, large variation of Lagrangian diffusion occur over mesoscale distances. It is found that high temporal resolution (3 h or less) is required for off-line transport calculations and that the reconstructions are sensitive to spurious motion in standard analysed winds.

1. Introduction

The distribution of chemical compounds in the atmosphere exhibits a large range of variability that is partly due to transport. This is particularly true in the lower stratosphere for species, like nitrous oxide N_2O which have no sources or sinks in this region. Ozone is chemically reactive in the lower stratosphere but its lifetime exceeds several weeks except in the regions where chlorine is activated within the winter polar vortex; that is long enough for transport to be effective.

In the lower stratosphere, vertical motion is limited by stratification to be of the order of 1 K/day in potential temperature. Hence is takes about 3 weeks to travel over a vertical distance of 1 km and transport is mostly dominated by horizontal motion. With a vertical shear $\Lambda \approx 2\,10^{-3}\,s^{-1}$ and a horizontal strain $\gamma \approx 10^{-5}\,s^{-1}$, a compact cloud of particles is first dispersed by vertical shear during a few hours until it reaches an equilibrium slope of $\Lambda/\gamma \approx 200$ within one day after which dispersion is mainly due to the horizontal strain (Haynes and Anglade, 1997). Under the repeated action of strain and foldings due to the nonlinearity of the flow, tracers are stirred and form a number

ACPD
4, 8285–8325, 2004

of sloping sheets which are observed as laminae in vertical soundings and aircraft transects. The core of intense jets, such as that circumventing the stratospheric polar vortex, acts as a transport barrier and is often associated with strong tracer gradient.

The proof of this concept is provided by the ability to reconstruct the small-scale distribution of tracers by advection methods using analysed winds (Waugh et al., 1994; Sutton et al., 1994; Mariotti et al., 1997). The basis of these methods is that the operational analysis provided by the major weather centers resolve the wind structures responsible of transport. Hence, the tracer structures at scales smaller than the analysed wind are to some extent predictable by integrating backwards in time the advection equation (Methven and Hoskins, 1999). There is no contradiction here: the information about unresolved tracer scales is fully contained in the time series of wind fields.

Reconstruction by pure advection generates, however, an endless growing number of structures in the tracer field as the reconstructed time increases. In fact, mixing performed by small-scale turbulence, not represented in the analysed winds, limits the smaller scale that tracer sheets may sustain. Assuming that the small-scale turbulence is roughly isotropic, vertical mixing is the most effective process in providing a cut-off scale for the tracer sheets, the vertical cut-off being converted into an horizontal cut-off by the slope factor.

Small-scale turbulence is due to a number of instabilities, either local instabilities of the wind profile or breaking of vertically propagating gravity waves. It is believed to be patchy in space and time. Although more elaborate representations are available (e.g., Vanneste and Haynes, 2000), it seems reasonable to estimate the effect of turbulence as an ordinary vertical diffusion D.

The literature exhibits a variety of estimates of D ranging from $5\,m^2\,s^{-1}$ to $0.001\,m^2\,s^{-1}$. The largest values are obtained from radar measurements assuming homogeneous turbulence near critical Richardson number (Woodman and Rastogi, 1984; Fukao et al., 1994; Nastrom and Eaton, 1997). These values are contradicted by recent estimates from high resolution balloon data (Alisse et al., 2000) and by stud-

ies of large-scale advective stirring (Waugh et al., 1997; Balluch and Haynes, 1997) that provide values in the lower part of the range, of the order of 0.01 $m^2 s^{-1}$ or less.

Both estimates of Waugh et al. (1997) and Balluch and Haynes (1997) were based, like the present study, on the dominating layer-wise motion in the stratosphere to generate tracer sheets. From the assumption that tracer structures are sloping sheets, Balluch and Haynes (1997) reduced locally the advection and the diffusion of a tracer to a one dimensional equation projected on an evolving gradient direction. They estimated an upper limit on vertical diffusivity by reconstructing several laminae selected from N_2O airborne measurements, varying the diffusivity until the reconstruction best agrees with the observations. In this study, we go a step further by removing any assumption about tracer distribution and using a powerful method to solve locally the advection-diffusion problem.

This new approach has been introduced in Legras et al. (2003) to study vertical diffusivity from the reconstruction of vertical ozone profiles. The conclusion of this study was to put an upper limit of 0.1 $m^2 s^{-1}$ for the vertical diffusivity in the lower stratosphere mid-latitude surf zone during winter. The possibility to test smaller values of the diffusivity was, however, impaired by the limited vertical resolution of ozone soundings with standard chemical sondes that is of the order of 100 m if we stay on the optimistic side. Using the slope factor 200, the equivalent horizontal resolution of ozone soundings does not exceed 20 km, while airborne tracer measurements are currently performed with resolution under 1 km for species like O_3, CH_4 or N_2O that can be measured at high frequency of one to a few Hertz. Hence, airborne measurements resolve at least 20 times better the small-scale sloping structure than standard ozone soundings. The above motivates the present study which extends Legras et al. (2003) by analysing airborne transects collected by the instruments on board the NASA ER-2 during the SOLVE campaign in the Arctic in January–March 2000.

Section 2 presents the method used for the Lagrangian reconstructions based on the advective-diffusive equation. Section 3 describes the data and trajectory calculations used in this study. Section 4 demonstrates that diffusive reconstructions of a tracer

ACPD
4, 8285–8325, 2004

are strikingly stable over a large range of reconstruction times. Section 5 defines the roughness criterion used to fit the vertical diffusion in this study. Section 6 discusses the reconstructions of the most significant SOLVE flights and the best fitting diffusivities; Sect. 7 discusses local structures. Section 8 discusses the relation between diffusivity and dispersion. Section 9 shows the spurious effects of under-resolving the temporal variations of the wind. Finally, Sect. 10 offers further discussion and conclusions.

2. Diffusive reconstruction

The standard reconstruction method for the mixing ratio of a tracer at time t_0 over a given domain $\mathcal{D}$ consists in finding the location at an earlier time $t_0-\tau$ of the parcels filling $\mathcal{D}$ at time t_0 and to attribute a mixing ratio to each parcel according to the tracer mixing ratio at its initial location at time $t_0-\tau$. The initial location is found by backward integration of the particle advection equation $d\boldsymbol{x}/dt=\boldsymbol{u}(\boldsymbol{x},t)$ where the wind $\boldsymbol{u}(\boldsymbol{x},t)$ is provided by interpolating in time and space the analysed winds provided by operational weather centers. The main interest of this calculation is that the reconstructed field at time t_0 gives access to much smaller scales than the initialisation field used at time $t_0-\tau$. In many previous studies, the tracer was potential vorticity (PV) and it was initialised according to the analysis from weather centers. The value of this approach has been demonstrated by comparing the reconstructed PV with observations of tracers, either in the stratosphere with aerosols and ozone (Waugh et al., 1994; Sutton et al., 1994; Mariotti et al., 1997; Orsolini et al., 2001) or in the troposphere with water vapour (Appenzeller et al., 1996). However, PV can hardly be measured by in situ instruments and cannot be assumed to correlate perfectly with any measurable tracer. Hence, recent efforts have been devoted to the direct reconstruction of observable chemical field. The tracer distribution at time $t_0-\tau$ is then provided, with a crude resolution, either by a chemical transport model (Legras et al., 2003) or by satellite observations (Orsolini et al., 2001).

The standard reconstruction method is fully deterministic. It fails to take into account

ACPD
4, 8285–8325, 2004

any diffusive process and generates a number of small-scale structures that increases exponentially with the reconstruction time τ. It is usually admitted that, according to the resolution of initial fields, reconstructions should be performed over durations of 10 to 20 days in the lower stratosphere (Methven and Hoskins, 1999; Waugh and Plumb, 1994) beyond which the number of spurious structures pervades the results.

In our approach, as sketched in Fig. 1, diffusion is taken into account by splitting the parcel at time t_0 into N particles which are all advected backward in time by the equation

$$\delta \boldsymbol{x} = \boldsymbol{u}(\boldsymbol{x}, t)\delta t + \boldsymbol{k}\delta\eta(t)\,, \tag{1}$$

where $\boldsymbol{k}$ is the vertical unit vector and $\delta\eta(t) \equiv w(t)\delta t$ is the product of a white noise process $w(t)$ by the time step δt. The white noise process is without memory (i.e. it is δ-correlated in time), and with a zero mean. In the limit $\delta t \rightarrow 0$ and after statistical average over a large number of particles, this is equivalent to adding a diffusion D to transport with

$$D = \frac{1}{2} < w^2 > \delta t\,. \tag{2}$$

In order to ensure that vertical velocities are bounded, we use a white noise based on a random variable r that is uniformly distributed over the interval $[-\sqrt{3}, \sqrt{3}]$ with zero mean and unit variance. Applying Eq. (2), the random process is then $\delta\eta = r\sqrt{2D\delta t}$ with a new drawing of r at each time step and for each particle. Actually, we use a time-step of 9 s for the random term which is one hundred times smaller than the time-step for advection in order to enhance statistical convergence.

The reconstructed mixing ratio of the parcel is the average of the mixing ratios of the N particles initialised at time $t_0 - \tau$.

The method just described is directly related to the solution of the advective-diffusive equation for a passive tracer C as

$$C(\boldsymbol{x}, t) = \int G(\boldsymbol{x}, t; \boldsymbol{y}, s) C(\boldsymbol{y}, s) d^3\boldsymbol{y}, \tag{3}$$

where $G(\boldsymbol{x}, t; \boldsymbol{y}, s)$ is the Green function describing the probability of a parcel that was in $\boldsymbol{y}$ at time s to be in $\boldsymbol{x}$ at time t. The Green functions satisfies the two equations

$$\frac{\partial G}{\partial t} + \boldsymbol{u}(\boldsymbol{x}) \cdot \nabla_x G = D\nabla_x^2 G \tag{4}$$

$$\frac{\partial G}{\partial s} + \boldsymbol{u}(\boldsymbol{y}) \cdot \nabla_y G = -D\nabla_y^2 G \tag{5}$$

with the initial condition $G(\boldsymbol{x}, t; \boldsymbol{y}, t) = \delta(\boldsymbol{x} - \boldsymbol{y})$. Here, the derivatives are taken with respect to the final coordinates $\boldsymbol{x}$ and t for the first equation and with respect to the initial coordinates $\boldsymbol{y}$ and s for the second one. The statistical average of mixing ratio over random backward trajectories is equivalent to solving Eq. (5). The negative sign in front of the diffusive term on the r.h.s. of Eq. (5) means that this equation is well-posed for backward integration in time.

Notice that the random process entering the advection equation has been described here assuming that time-stepping is performed using a simple Euler scheme. More sophisticated numerical schemes require adequate transformations.

3. Data and trajectory processing

Data have been collected by NASA ER-2 aircraft during SOLVE campaign from January to March 2000. The ER-2 is equipped with a number of instruments performing in situ measurements of chemical tracers. We have used the unified nitrous oxide data combining the measurements of three instruments (ACATS, ARGUS, ALIAS) at 0.33 Hz with a resulting relative precision of 3 ppbv (1.5%) at flight level (Hurst et al., 2002) and the NOAA ozone photometer with 1 Hz frequency and a relative precision of 10 ppbv (0.5%) (Proffitt et al., 1989). During the SOLVE campaign, eleven flights were performed from Kiruna (67.83° N, 20.42° E) which was located inside the polar vortex during most of the winter. We have processed ten of the flights during which all the relevant instruments were operating. Except for two dates on 27 January 2000 and 11

March 2000, the ER-2 flights were performed entirely inside the polar vortex and measured fairly homogeneous mixing ratios of N_2O and O_3 over constant pressure level legs, indicating that the vortex was well mixed and homogenized during this period. Indeed, the Arctic winter 2000 has been remarkably cold with only a minor warming in early February and no major warming until mid-March (Rex et al., 2002). We have also used the transit flights from Kiruna to California on 16 March 2000 and 18 March 2000 during which the instruments were operating in order to compare turbulent diffusivity within the vortex and the mid-latitude surf zone.

Reverse integrations of particles trajectories initialised along each transect have been performed with TRACZILLA, a modified version of the trajectory code FLEXPART (Stohl et al., 2002) which uses ECMWF (European Center for Medium range Weather Forecast) winds at 1° horizontal resolution and on 61 hybrid levels with 3-h resolution by combining analysis available every 6 h with first guesses at intermediate times. The modifications from FLEXPART advection scheme consisted mainly in discarding the intermediate terrain following coordinate system and performing a direct vertical interpolation of winds, from hybrid levels, which is linear in log-pressure. The vertical velocity used in this study is computed by the FLEXPART preprocessor using a mass conserving scheme in the hybrid ECMWF coordinates. A small correction due to a missing term in FLEXPART has been introduced but it has virtually no impact. The model uses a fixed time step of δt=900 s. Halving it has no impact on our results. Unless stated differently, the reconstruction are performed by releasing N=1000 particles every 4 s along the flight track using the GPS ER-2 data to locate the release points, that is about with the same frequency than the N_2O measurements.

Assignment of N_2O and O_3 was performed from $t_0-\tau$ location from three-dimensional fields produced by REPROBUS (REactive Processes Ruling the Ozone BUdget in the Stratosphere). REPROBUS is a three-dimensional chemical-transport model (CTM) with a comprehensive treatment of gas-phase and heterogeneous chemical processes in the stratosphere (Lefèvre et al., 1994, 1998). Long-lived species, including ozone, are transported by a semi-Lagrangian scheme (Williamson, 1989)

forced by the 6-hourly ECMWF wind analysis. The model is integrated on 42 levels hybrid pressure levels that extend from the ground up to 0.1 hPa, with a horizontal resolution of 2°. For the experiments presented here REPROBUS was initialised on 15 October 1999. Chemical species (including N_2O) were initialised from October zonal means obtained after a 5-year simulation driven by GCM winds. The ozone field was reinitialised on 1 December 1999 from the three-dimensional O_3 analysis computed at ECMWF.

4. Tracer reconstruction from random trajectories

Figure 2 shows how the diffusive reconstruction differs from the standard single particle deterministic reconstruction. The particles emitted from a single point and diffused backward spread spatially as seen in the upper panel. Hence they sample a range of N_2O values at the initial locations. This sampling varies much less from one point to the next than any individual trajectory, thus providing a much smoother reconstruction, as seen in the lower panel. The diffusive reconstruction is not, however, just a smoothed version of the single particle reconstruction. This latter should be seen as one possible realisation among many that contributes to the statistical average of the diffusive reconstruction. The small wiggles on the deterministic reconstruction are fluctuations due to the finite sampling of N particles per point. Their amplitude is proportional to $\sqrt{D/N}$.

The first panel of Fig. 3 shows N_2O observed by the ER-2 and as predicted by REPROBUS along the track of the 11 March 2000 flight along Norvegian coast that crossed the polar vortex edge at about 11:00 UT and crossed it back at about 13:00 UT. A sheet of polar air, marked on the figure, was crossed on both ways just outside the vortex edge. REPROBUS over predicts N_2O by about 50% within the vortex but provides a good fit to the observations within the surf zone. Owing to its low spatial resolution, it fails, however, to reproduce the large gradients at the vortex edge and the

ACPD
4, 8285–8325, 2004

sheet of polar air. The following panels of Fig. 3 show the diffusive reconstructions of N_2O with D=0.01 $m^2\,s^{-1}$ and for increasing values of τ. For small τ=2 days, the reconstructed curve does not differ strongly from REPROBUS prediction, but already exhibits lower values within the vortex. At τ=7 days, the vortex edge is well defined and the polar air sheet starts to emerge. The sheet is well formed at τ=11 days and a number of other details emerge. By τ=24 days the reconstructed curve has reached a stable shape for all details that changes only weakly and slowly as τ is further increased. The calculation comes up to τ=147 days, that is more than 4 months, using an initialisation date before the onset of the polar vortex. The sole visible effect of increasing τ to large values seems to be a uniform slow decrease of N_2O within the polar vortex.

Hence, unlike single trajectory reconstruction, diffusive reconstruction is to a large extent insensitive to the reconstruction time τ. This latter must be larger than an offset time required to generate large amplitude gradient from the smooth tracer field used at the initial time. The insensitivity to τ arises from the fact that Eq. (3) is valid for any time s and that N_2O is basically transported by REPROBUS too.

In the absence of diffusion, tracer gradients are expected to grow exponentially in time at a rate given by the average isentropic strain (Haynes and Anglade, 1997). With diffusion, the size of tracer jumps is bounded by $\sqrt{\gamma_{max}/D}$ where γ_{max} is the maximum strain. Hence, the offset time is expected to depend weakly on D, as $\ln D$. It is also clear that the Green function dependence on $\boldsymbol{y}$ in Eq. (3) gets smoother as τ=t−s increases, and consequently that the reconstruction is only sensitive to the largest scales of the initial tracer distribution when τ is large. A more complete discussion of the predictability of tracer gradients is deferred to another work.

Reconstructions of O_3 are shown for comparison in Fig. 4. Unlike N_2O, O_3 is not a conserved tracer within the polar vortex where it is depleted by chlorine catalyzed chemistry. During March 2000, REPROBUS has not been able to destroy enough ozone inside the polar vortex, hence the large deviation observed on the left panel of Fig. 4. This effect is accented in our calculation which does not take into account any chemistry and reconstructed O_3 exhibits a sustained backward growth as τ increases.

ACPD
4, 8285–8325, 2004

The fluctuations are, however, preserved like for N_2O.

5. Roughness

As the goal of this study is to estimate turbulent diffusivity, we need to compare fluctuations in the observed and reconstructed tracer transects. A first way, already followed by Waugh et al. (1997) and Balluch and Haynes (1997), is to identify some structures, like the sheet of polar air already mentioned, and to adjust the diffusion to provide the best fit of reconstruction to observations. This will be used below but it is not always possible to identify such structures, especially when stirring is strong. If we give up this idea, a second way consists in using a statistical measure of the fluctuations as a basis for the comparison. In Legras et al. (2003), comparisons based on spectra and increment variance have been discussed but these measures are sensitive to the small-scale noise and need to be applied to a pre-filtered signal. Legras et al. also introduced a new measure called the "roughness function". We refine here this notion to take into account the small-scale instrumental noise without need to pre-filter the signal.

Our definition of roughness is provided by the following algorithm for a discrete curve described by a list of K points (x_i, y_i) with an assumed uncertainty $\pm\sigma$:

1. For each value of $p>0$ and for each value $x_c=x_i$, $y_p^+(x_i)$ is defined as the smallest y_c such that the parabola $2p(y-y_c)=(x-x_c)^2$ lies entirely above the curve joining the points $(x_i, y_i-\sigma)$.
2. Similarly, $y_p^-(x_i)$ is defined as the largest y_c such that the inverted parabola defined with p turned into $-p$ lies entirely below the curve joining the points $(x_i, y_i+\sigma)$.
3. The two osculating curves $y_p^+(x_i)$ and $y_p^-(x_i)$ are then used to define the "roughness function" $\phi(p)=\frac{1}{K}\sum_{i=1}^{K}\max(0, y_p^+(x_i)-y_p^-(x_i))$.

ACPD
4, 8285–8325, 2004

An arbitrary rescaling of the units of x_i and y_i preserves the parabolic shape and is equivalent to multiply p by a constant. Figure 5 illustrates the algorithm, showing that the roughness function is the positive area between two shifted osculating curves. The dependence of roughness upon scale is described by varying p with multiplicative steps. It can be shown that calculating the osculating curves reduces to a Legendre transform which is performed using a fast algorithm (Lucet, 1997).

6. Analysis of SOLVE flights

We first present a detailed analysis of the 27 January 2000 flight which spans both the inside and the outside of the vortex and displays a number of interesting structures. Figure 6 shows the measured and reconstructed transects for 27 January 2000 with three values of D for both N_2O and O_3 and τ=38 days. It also shows a non-diffusive reconstruction at the same τ for comparison.

The REPROBUS model provides a good large-scale fit to the observations for N_2O. Predicted ozone is slightly larger than observed inside and outside the vortex. The edge of the polar vortex is well identified on the measured and reconstructed N_2O transects, but is hardly seen on the O_3 transects. It shows up very well, however, on the variance for reconstructed O_3 which undergoes a sudden jump on the edge; the N_2O variance has also much larger fluctuations outside the vortex than inside and peaks on the edge but does not exhibit a jump profile. Several structures have been marked in the measured and reconstructed transects. The first one (black) is a local N_2O decrease and O_3 along the edge, probably due to enhanced descent (Mariotti et al., 2000); the second one (magenta) is a spell of fluctuations outside the vortex and the third one (green) is presumably the trace of a filament expelled from the polar vortex. For all these structures, the two smallest values of D reconstruct excessive amplitude with respect to the observations and $D \approx 0.1\,m^2\,s^{-1}$ provides a better fit. It is also clear that the edge of the polar vortex is too steep for the two smallest values of D. Hence, on the edge and outside the polar vortex, the turbulent diffusion must be fairly

large to account for the observed structures.

It is more difficult to associate observed and reconstructed structures inside the vortex for time t>13 h but the visual analysis now reveals that D=0.1 m^2 s^{-1} reconstructs a too smooth transect compared to the observation, suggesting that turbulent diffusion is smaller inside the vortex. Taking this into account, roughness has been calculated separately inside and outside the vortex (removing also the dive section) and also for two different values of the offset, one and two times the precision. The two families of roughness curves displayed in Fig. 6 show that the small-scale fluctuations, for both N_2O and O_3, scale best in agreement with $D\approx$0.1 m^2 s^{-1} outside the vortex and with $D\approx$0.001 m^2 s^{-1} inside. The inside value, which is indeed very small, must be tempered by the small length of the branch inside the vortex during this flight.

The 27 January 2000 flight is, however, the only one to exhibit a significant level of tracer fluctuations inside the polar vortex. All the 8 flights done entirely within the polar vortex exhibit very few tracer fluctuations when the ER-2 flies on level legs (on a slightly climbing trajectory actually) as if the vortex was very well mixed during this winter except for a few minor intrusions (Jost et al., 2002) or anomalous diabatic events. In fact, strong sudden warmings which are the main source of variability within the vortex did not occur during 2000 Arctic winter before mid-March. As a result, the comparison of observed and reconstructed transects is also a test for the transport errors due to the analysed winds used in the reconstruction. Figure 7 compare observed and reconstructed transects for 7 March 2000. The observed transects for both N_2O and O_3 do not exhibit any other structures than small-scale fluctuations over the constant level legs. These fluctuations exceed only occasionally the precision for N_2O but can be considered as significant for O_3 which is measured with better accuracy. It is also visible from the N_2O reconstruction that the reconstruction enhances a number of structures at scales larger than 100 km (about 8 min of flight) that are absent from the observations. By the cascade process of chaotic advection, these structures generate small-scale fluctuations requiring a diffusivity $D\approx$0.1 m^2 s^{-1} to fit the roughness of the observations. The O_3 reconstruction does not exhibit the same amount of spurious mesoscale

structures as N_2O and hence generates less small-scale structures, resulting into a value of $D \approx 0.01\,m^2\,s^{-1}$ fitting observed roughness. Our interpretation of this discrepancy is that the spurious structures in the N_2O reconstruction are due to spurious vertical transport in the vertical N_2O gradient and that the lower sensitivity of O_3 is due to its weaker vertical gradient measured by the height-scale $\partial[O_3]/\partial p/[O_3] \approx 128\,hPa$ compared to 56 hPa for N_2O at 60 hPa inside the polar vortex in early March.

Table 1 summarizes the estimates of D based on roughness for N_2O and O_3, and checked by visual inspection, for all the flights of the SOLVE campaign from Kiruna. It is visible that previous results are mostly confirmed during the whole campaign with the noticeable exception of 11 March 2000 flight during which fairly small diffusion was observed outside the polar vortex in the N_2O reconstructions.

Finally, Fig. 8 compares observed and reconstructed transects for the return flight of 16 March 2000 from Kiruna to North America, that occurred entirely outside the vortex and confirms the estimate $D \approx 0.1\,m^2\,s^{-1}$ in the surf zone.

7. Local variations of diffusivity

As already noticed in Sect. 4, the 11 March 2000 flight crossed a sheet of polar air at some distance outside the vortex edge. This sheet is the remain of a fairly broad streamer emitted from the vortex by 28 February 2000, 13 days earlier. On 11 March, its signature was very faint in the ECMWF analysed potential vorticity (not shown) but it was still very well preserved in the N_2O field. Its weak signature in the O_3 field is due to the weak horizontal O_3 gradient in the region where it originates from.

Figure 9 shows an enlargement of the sheet crossing for the observed and reconstructed transects. The flight was mainly along mean gradient and the observed sheet was met 325 km after crossing the vortex edge. The sheet is 120 km large and the striking feature is the asymmetry of its two edges. The south edge is smooth and fits very well an error function with width 32 km. The north edge is steep with a width of about 2.5 km. The reconstruction succeeds in reproducing the sheet albeit it is slightly

ACPD
4, 8285–8325, 2004

displaced southward by 104 km but the asymmetry of the sheet cannot be reproduced with a single value of the diffusivity which generates the same slope on both edges. The observed south slope 1.49 ppbv km^{-1} lies between that for D=0.1 and 0.01 m^2 s^{-1}, respectively 1.22 and 2.64 ppbv km^{-1}, closer to the first one. The observed north slope is as steep as that for D=0.001 m^2 s^{-1}. Hence, a variation of more than one order of magnitude for the Lagrangian turbulent diffusion occurs over a short distance of about 100 km across the sheet.

It would not be surprising to observe such variations in the instantaneous turbulent diffusion which is expected to be very intermittent in time and space. The persistence of sharp variations in the averaged Lagrangian diffusivity indicates the presence of a transport barrier.

8. Relation between diffusion and dispersion

A convenient way to parameterize turbulent diffusion is to assume a relation between dispersion and turbulent diffusion as initially done in Prandtl's mixing length hypothesis and in more refined models like Smagorinsky parameterization (see, e.g., Pope, 2000). In the transport model CLAMS (McKenna et al., 2002; Konopka et al., 2004), mixing is parameterized as a function of the deformation of a grid of points advected by the flow.

Since turbulent diffusion is estimated here independently of any relation with dispersion, it is interesting to compare both quantities.

8.1. Onset of dispersion

First we check that the consistency of our numerical calculations with respect to the dynamics of advection and diffusion. Starting from a spatial δ-distribution, diffusion initially dominates and the inertial axis of the cloud of N particles grow as $D^{1/2}t^{1/2}$. This applies here to all axes even if diffusion only acts in the vertical direction because the time step δt is such that $\Lambda\delta t$=O(1). This first stage ends when the cloud reaches a

size ℓ_d scaling as $D^{1/2}\gamma^{-1/2}$ for which diffusion equilibrates with strain in one direction, after which expansion of the cloud pursues exponentially with a rate of the order γ as a pancake or a filament (depending on the number of unstable directions) while the smaller transversal dispersion remains of the order of ℓ_d.

The duration t^* of the first stage satisfies $D^{1/2}t^{*1/2}\sim D^{1/2}\gamma^{-1/2}$ and hence should be independent of D. This is checked in Fig. 10 showing the growth of the inertial volume for a wide range of diffusivity values. The diffusive stage for all cases ends at the same $t^*\approx 3$ days. The subsequent growth rate of the inertial volume is bounded by two curves showing the 5% and 95% percentiles of the distribution. The growth is exponential as long as the largest size of the cloud remains small with respect to the characteristic scale of strain variation and the cloud retains an ellipsoidal shape. This linearity condition is more easily satisfied for the 5% percentile which corresponds to a growth rate of 0.26 days^{-1}. The upper 95% percentile grows initially at a higher rate of 0.63 days^{-1}. For the two largest diffusions tested here, the size of the cloud rapidly violates the linearity condition and growth weakens as the cloud distorts and mixes with itself.

8.2. Lyapunov exponents

A geometric measure of deformation induced by strain are Lyapunov exponents (Pierrehumbert and Yang, 1993). For non diffusive motion, they describe the transformation of an infinitesimal spherical cloud surrounding a particle at time t_0 into an ellipsoid at time t_1 in a local reference frame relative to the particle. If $\delta\boldsymbol{x}(t)$ is an infinitesimal deviation at time t, its evolution is described by the tangent linear operator $\mathbf{M}$ as $\delta\boldsymbol{x}(t_1)=\mathbf{M}(t_0,t_1)\delta\boldsymbol{x}(t_0)$ and the local finite-time Lyapunov exponents λ_i are related to the eigenvalues σ_i of $\mathbf{M}^t\mathbf{M}$ by $2\lambda_i=1/(t_1-t_0)\ln\sigma_i$. A convenient way to calculate the local Lyapunov exponents is by finite difference using a small initial perturbation in three orthogonal directions and performing at regular intervals an estimate of the growth of length, surface and volume, followed by an orthonormalization procedure that regen-

ACPD
4, 8285–8325, 2004

erates an initial triedron for the following interval (for more details, see Benettin et al., 1980; Ott, 1993). It can be shown (Goldhirsch et al., 1987) that, after a transient time, this method provides the three local Lyapunov exponents $\lambda_1 \geqq \lambda_2 \geqq \lambda_3$. Since **M** can be calculated as a by-product of the procedure for short times, it has been checked that this is true for $t_1 - t_0 > 20$ days. The norm used in the orthogonalization takes into account the aspect ratio of stratospheric structures by magnifying the vertical direction by a factor Λ/γ with respect to the horizontal directions. The Lyapunov exponent are calculated over the duration τ (that is $\tau = t_1 - t_0$) near the single trajectory obtained for $D=0$ and the orthogonalization interval is one day.

For backward evolution in time, the smallest exponent λ_3 describes the exponential elongation of line segments, while $\lambda_1 + \lambda_2$ describes the growth rate of surface elements and $\lambda_1 + \lambda_2 + \lambda_3$ describes the growth rate of the volume. Since the flow is close to incompressible, the sum of the three exponents should be close to zero. Three cases can hold:

1. $\lambda_1 \approx \lambda_2 > 0$ and $\lambda_3 \approx -\lambda_1 - \lambda_2$ which means that sheets are formed if $t > 0$ and filaments if $\tau < 0$.

2. $\lambda_1 > 0$ and $\lambda_2 \approx \lambda_3 < 0$ which means that sheets are formed if $t < 0$ and filaments if $\tau > 0$

3. $\lambda_1 > 0$, $\lambda_2 \approx 0$ and $\lambda_3 \approx -\lambda_1 < 0$ which means that filaments are formed forward and backward in time.

For diffusive motion and backwards in time, the negative exponents describe the elongation of the cloud of particles emitted from each point for $|\tau| > t^*$.

Figure 11 shows the N_2O reconstruction and Lyapunov exponent for 11 March 2000 and $\tau = 32$ days. Since the calculation is based on single deterministic trajectories, the Lyapunov exponents are noisy but several properties can be drawn from the figure. There is a clear separation in magnitude between the inside of the polar vortex, with typical values smaller than 0.1 day^{-1} and small variance, and the outside, with typical

ACPD
4, 8285–8325, 2004

values of the order of 0.25 day^{-1} and large deviations. Hence, the inside of the polar vortex is much less strained than the outside. Larger dispersion, especially in the vertical, means sampling a wider range of N_2O values and, hence, the variance is also larger outside the polar vortex than inside. The unfiltered curves of the most negative Lyapunov exponent and the variance are anti correlated with a coefficient −0.407 which is significant since it is calculated over 8844 points along the flight. The sum of the three Lyapunov exponents is close to zero. In principle, its variation should correlate with the variation of parcel density which can be calculated but we reach here the limit of our numerics and the correlation is very poor. The sign of the intermediate Lyapunov oscillates around 0 along the flight implying the formation of sheets and filaments depending on the location.

Figure 12 shows an enlargement around the sheet of polar air. The small dispersion that characterizes the polar air has been preserved inside the sheet in agreement with its isolation from surrounding air. Two maxima are observed on both edges indicating that strong shear, presumably due to PV jump, has been experienced by the parcel over the last three weeks but there is no distinction between the smooth and the sharp edge. This is perhaps an indication that the event that led to the smooth south edge is not due to shear induced turbulence but rather to an exterior event such as breaking gravity waves, not unlikely to occur along the cost of Scandinavia.

9. Sensitivity to temporal resolution

Our reconstructions are based on using 3-hourly winds obtained by interleaving first guesses with ECMWF analysis. This is the standard procedure implemented in FLEXPART (Stohl et al., 2002) and inherited in TRACZILLA. A number of other Lagrangian studies in the literature have used instead 6-hourly winds based solely on analysis. The main reason for this choice seems practical since the ECMWF 6-hourly analysis or reanalysis are mirrored and easily available from many locations. It is, however, questionable that the 6-h archiving period, which has been chosen to provide accu-

rate climatology, is optimum to perform off-line transport calculations. This led us to investigate the effect of changing the temporal resolution of advecting winds onto the reconstruction and estimated turbulent diffusion. An other motivation was a recent work (Stohl et al., 2004) showing that forecasted winds are much less diffusive than analysis. Hence, we have also tested the effect of replacing analysed winds by forecasted winds.

We have thus performed a series of reconstructions for the same case, namely that of 11 March 2000 which is already well documented in this study and for a single value of diffusivity D=0.01 $m^2 s^{-1}$ by varying the field of advecting winds. The reference reconstruction, shown in Fig. 13b is that performed with 3-hourly winds, one-degree horizontal resolution and 60 hybrid levels in the vertical. Figure 13c shows the reconstruction obtained by halving the horizontal resolution of advecting winds to 0.5°. The reconstruction is strikingly insensitive to this spatial refinement in agreement with previous observations (Waugh and Plumb, 1994; Methven and Hoskins, 1999) and the fact that ECMWF analysed winds bear little variance at such small scales in the lower stratosphere. Notice also that near the pole the 1° longitude-latitude grid already over-resolves the longitudinal variations. Figure 13d shows the reconstruction obtained by calculating transport from interpolated 6-hourly analysed winds, dropping the first guesses out of our procedure. The effect is this time dramatic with a strong enhancement of the fluctuations inside and outside the polar vortex. The sheet is still visible but can easily be confounded with other spurious structures. In order to dwell into the source of this considerable deterioration, we have performed a reconstruction using two-day forecasts, namely we use the 48- and 54-h forecasts from the deterministic forecast runs performed every 12 h at ECMWF. Figure 13e is constructed from this new 6-hourly dataset. With respect to Fig. 13c, the reconstruction shows a considerable damping of the fluctuations and much better agreement with the observations. We could not test the reconstruction with 3-hourly forecasts since they have not been archived at ECMWF before 2002. Finally, Fig. 13f shows the reconstruction obtained from 3-hourly winds taken from the ERA40 reanalysis instead of the operational anal-

ACPD
4, 8285–8325, 2004

ysis. The reconstruction differs from the reference but rivals in skill compared to the observation with the noticeable exception of the polar air sheet which is badly predicted.

These results indicate that off-line transport calculations are highly sensitive to the lack of resolution of the wind fluctuations in 6-hourly analysis. Whatever the true timescale of a given fluctuation, sampling the wind field every x hours makes it persistent over x hours. Fluctuations are mostly seen in the vertical wind calculated from the divergence field, notoriously noisy in the analysis, using the mass conservation. As a result, vertical displacements are overestimated and in turn, diffusive transport along vertical tracer gradients is also overestimated. In the limit of very short-lived fluctuations, it can be shown easily that vertical diffusive transport is proportional to the sampling interval. For our prospect of measuring turbulent diffusion, the excess transport requires to overestimate Lagrangian diffusion in order to smooth out the excess fluctuations in the reconstructed tracer.

Not only the fluctuations in the 6-hourly winds are under sampled, they are also to a large extend spurious as demonstrated from the comparison between analysed and forecast winds. In spite of the efforts to filter out gravity waves during initialisation, the analysed wind contain a significant level of spurious motion which is damped during the forecast as the model relaxes to its attractor (Kalnay, 2003). This spurious motion presumably consists mainly in short-period gravity waves. Wavy structures with scales of the order of several tens to a few hundreds km are often seen over the displacements of the cloud of parcels emitted from a single location or even in the reconstruction itself. Figure 14 shows such an example.

However, it is still unclear whether 3 h (the maximum frequency at which wind datasets are currently available) is a sufficiently short interval to achieve satisfying reconstructions. In fact, the discrepancy between estimates of D from N_2O and O_3 inside the vortex indicate that this is not the case and that our estimate of D is still an upper bound of the true value representing unresolved turbulent motion.

10. Conclusions

We have shown that the sensitivity of Lagrangian reconstruction to the integration time of back-trajectories disappears when diffusion is added as a random walk over an ensemble of trajectories and reconstruction is based on statistical average over this ensemble. Using the tracer field produced by REPROBUS as initialisation, it takes 2 to 4 weeks for diffusivity varying from $0.1\,m^2\,s^{-1}$ to $0.001\,m^2\,s^{-1}$ to reach a stage where small-scale structures are essentially invariant under extension of the reconstruction time.

The comparison of ER-2 measurements of N_2O and O_3 with reconstructions performed with varying diffusivity provides an estimate of turbulent diffusivity of the order of $0.1\,m^2\,s^{-1}$ in the surf zone and one order of magnitude less at least inside the polar vortex, based on the statistical distribution of tracer fluctuations. When well-defined structures are identified in the observations and the reconstructions, a local estimate of diffusivity is possible and large variations of more than one order of magnitude have been observed across the width of a polar vortex sheet.

The dispersion measured by Lyapunov exponent is much reduced inside the polar vortex compared to outside. Hence models that parameterize mixing based on deformation, like CLAMS (Konopka et al., 2004) would correctly predict less mixing inside the polar vortex than outside. However, the absence of correlation between diffusion and dispersion on the two edges of the polar air sheet on 11 March 2000 is an indication that such parameterization may miss numerous mesoscale features.

The estimate of diffusivity within the surf zone is in agreement with previous results based on ozone sounding (Legras et al., 2003). The resolution of standard ozone soundings is so coarse that lower diffusivity could not be tested while the ER-2 data are providing a much higher resolution and are much better suited to study the small-scale fluctuations of tracers.

The reconstructions are found to be sensitive to the quality of the wind fields used for the advection. In particular, the ECMWF analysis seems to contain a significant amount

ACPD
4, 8285–8325, 2004

of short-lived fluctuations which induce spurious transport, especially if advecting winds are interpolated between 6-hourly standard ECMWF archived winds.

This spurious effect is probably also affecting transport in REPROBUS. For instance the overestimation of N_2O within the polar vortex on 11 March 2000 (see Fig. 3) is also found in the CLAMS model when mixing is set at a too high value (Konopka et al., 2004, Fig. 8). Our reconstruction based on 3-hourly winds reduces the spurious mixing and hence decreases the value of N_2O towards the observed value. The fact that slightly lower values than observed are obtained in Fig. 3i could be attributed to errors in the initial REPROBUS field or too strong diabatic descent within the vortex.

The turbulent diffusivity estimated in this study is the combination of the unresolved turbulent motion (the "true turbulent diffusivity") and the need to filter the spurious motion contained in the analysed winds. The second effect is likely to hinder the first one as suggested by the comparison of results obtained with N_2O and O_3. It is also possible that chemical reactions contribute to smooth the spatial fluctuations of O_3 but it is not easy to conceive a possible mechanism since depletion chemistry does not tend to relax O_3 to an equilibrium value and ClO fluctuations should rather increase the ozone fluctuations (Edouard et al., 1996).

Our results indicate that the state-of-the-art in off-line transport studies, which is mainly based on 6-hourly analysed winds, is far from being satisfactory. A significant improvement is provided by interleaving first guesses to provide 3-hourly winds but it is yet unclear that these winds do not contain significant aliases of high-frequency fluctuations, and hence are still inducing excess transport with respect to what would be found by performing on-line calculations. This latter solution does not seem practical with an operational weather forecast model but archiving winds at higher resolution could be considered, at least for test purpose over a limited period of time. Another possibility would be to archive time-averaged winds instead of instantaneous values. The fact that the high frequency fluctuations are to some large extend a spurious effect of the initialisation could be circumvented by using winds from short-time forecast with, sometimes, strongly improved results as shown in Fig. 13e. The effect of using 4-D-Var

ACPD
4, 8285–8325, 2004

analysis, operational at ECMWF after 2002, instead of 3-D-Var, should also in principle reduce the amount of spurious gravity waves in the analysis. Finally, a number of models, including CLAMS, are using in the stratosphere vertical winds calculated from the local heating rate and the vertical profile of potential temperature. Although such winds are not providing automatic mass conservation they seem to reconstruct better the observed tracer, at least in Fig. 12 of Konopka et al. (2004) for 7 March 2000. These questions will be investigated in further work.

Acknowledgements. We acknowledge D. F. Hurst, H.-J. Jost, E. C. Richards, C. R. Webster, J. W. Elkins, S. M. Schauffler and E. L. Atlas for provided data from ACATS, ARGUS, ALIAS, WAS and ozone instruments on board the ER-2 during the SOLVE campaign. We acknowledge A. Tuck for useful discussions and advices.

References

Alisse, J.-R., Haynes, P., Vanneste, J., and Sidi, C.: Quantification of stratospheric mixing from turbulence microstructure measurements, Geophys. Res. Lett., 27, 2621–3224, 2000. 8287

Appenzeller, C., Davies, H., and Norton, W.: Fragmentation of stratospheric intrusions, J. Geophys. Res., 101, 1453–1456, 1996. 8289

Balluch, M. and Haynes, P.: Quantification of lower stratospheric mixing processes using aircraft data, J. Geophys. Res., 102, 23 487–23 504, (97JD00607), 1997. 8288, 8295

Benettin, G., Galgani, L., Giagilli, A., and Strelcyn, J.-M.: Lyapunov characteristic exponents for smooth dynamical systems and for Hamiltonian systems; a method for computing all of them, I: Theory, Meccanica, 9–80, 1980. 8301

Edouard, S., Legras, B., Lefèvre, F., and Eymard, R.: The effect of small-scale inhomogeneities on ozone depletion in the Arctic, Nature, 384, 444–447, 1996. 8306

Fukao, S., Yamanaka, M., Ao, N., Hocking, W., Sato, T., Yamamoto, M., Nakamura, T., Tsuda, T., and Kato, S.: Seasonal variability of vertical eddy diffusivity in the middle atmosphere. Three-year observations by the middle and upper atmosphere radar, J. Geophys. Res., 99, 18 973–18 987, 1994. 8287

Goldhirsch, I., Sulem, P.-L., and Orszag, S. A.: Stability and Lyapunov stability of dynamical

systems: a differential approach and a numerical method, Physica D, 27, 311–337, 1987. 8301

Haynes, P. and Anglade, J.: The vertical-scale cascade of atmospheric tracers due to large-scale differential advection, J. Atmos. Sci., 54, 1121–1136, 1997. 8286, 8294

Hurst, D., Schauffler, S., Greenblatt, J., Jost, H., Herman, R., Elkins, J., Romashkin, P., Atlas, E., Donnelly, S., Podolske, J., Loewenstein, M., Webster, C., Flesch, G., and Scott, D.: Construction of a unified, high-resolution nitrous oxide data set for ER-2 flights during SOLVE, J. Geophys. Res., 107(D20), 8271, doi:10.1029/2001JD000417, 2002. 8291

Jost, H.-J., Loewenstein, M., Greenblatt, J., Podolske, J., Paul Bui, T., Hurst, D., Elkins, J., Herman, R., Webster, C., Schauffler, S., Atlas, E., Webster, C., Schauffler, S., Atlas, E., Newman, P., Lait, L., and Wofsy, S.: Miwxing events revealed by anomalous tracer relationships in the Arctic vortex during winter 1999/2000, J. Geophys. Res., 107(D24), 4795, doi:10.1029/2002JD002380, 2002. 8297

Kalnay, E.: Atmospheric Modeling, data assimilation and predictability, Cambridge Univ. Press, Cambridge, UK, 2003. 8304

Konopka, P., Steinhorst, H.-M., Grooß, J.-U., Günther, G., Müller, R., Elkins, J., Jost, H.-J., Richard, E., Schmidt, U., Toon, G., and McKenna, D.: Mixing and ozone loss in the 1999–2000 Arctic vortex: simulations with the three-dimensional Chemical Lagrangian Model of the Stratosphere (CLaMS), J. Geophys. Res., 109(D2), 2315, doi:10.1029/2003JD003792, 2004. 8299, 8305, 8306, 8307

Lefèvre, F., Brasseur, G. P., Folkins, I., Smith, A. K., and Simon, P.: Chemistry of the 1991–1992 stratospheric winter: Three-dimensional model simulations, J. Geophys. Res., 99, 8183–8195, 1994. 8292

Lefèvre, F., Figarol, F., Carslaw, K., and Peter, T.: The 1997 Arctic ozone depletion quantified from three-dimensional model simulations, Geophys. Res. Lett., 25, 2425–2428, 1998. 8292

Legras, B., Joseph, B., and Lefèvre, F.: Vertical diffusivity in the lower stratosphere from Lagrangian back-trajectory reconstructions of ozone profiles, J. Geophys. Res., 108, 4562, doi:10.1029/2002JD003045, 2003. 8288, 8289, 8295, 8305

Lucet, Y.: Faster than the Fast Legendre Transform, the Linear-time Legendre Transform, Numer. Algorithms, 171–185, 1997. 8296

Mariotti, A., Moustaoui, M., Legras, B., and Teitelbaum, H.: Comparison between vertical ozone soundings and reconstructed potential vorticity maps by contour advection with surgery, J. Geophys. Res., 102, 6131–6142, 1997. 8287, 8289

Mariotti, A., Mechoso, C., Legras, B., and Chi, Y.: The evolution of the ozone "collar" in the Antarctic lower stratosphere during early August 1994, J. Atmos. Sci., 57, 402–414, 2000. 8296

McKenna, D., Konopka, P., Grooß, J.-U., Günther, G., Müller, R., Spang, R., Offermann, D., and Orsolini, Y.: A new Chemical Lagrangian Model of the Stratosphere (CLaMS): 1. Formulation of advection and mixing, J. Geophys. Res., 107(D16), 4309, doi:10.029/2000JD000114, 2002. 8299

Methven, J. and Hoskins, B.: The advection of high-resolution tracers by low-resolution winds, J. Atmos. Sci., 56, 3262–3285, 1999. 8287, 8290, 8303

Nastrom, G. and Eaton, F.: Turbulent eddy dissipation rates from radar observations at 5–20 km at White Sand missile range: New Mexico, J. Geophys. Res., 102, 19 495–19 505, 1997. 8287

Orsolini, Y., Hansen, G., Manney, G., Livesey, N., and Hoppe, U.-P.: Lagrangian reconstruction of ozone column and profile at the Arctic Lidar Observatory for Middle Atmosphere Research (ALOMAR) throughout the winter and spring of 1997–1998, J. Geophys. Res., 106, 10 011–10 021, 2001. 8289

Ott, E.: Chaos in dynamical systems, Cambridge Univ. Press, 1993. 8301

Pierrehumbert, R. and Yang, H.: Global chaotic mixing on isentropic surfaces, J. Atmos. Sci., 50, 2462–2480, 1993. 8300

Pope, S.: Turbulent Flows, Cambridge University Press, 770, 2000. 8299

Proffitt, M., Steinkamp, M., Powell, J., McLaughlin, R., Mills, O., Schmeltekopf, A., Thompson, T., Tuck, A., Tyler, T., and Winkler, R.: In situ ozone measurements within the 1987 Antarctic ozone hole from a high-altitude ER-2 aircraft, J. Geophys. Res., 94, 16 547–16 555, 1989. 8291

Rex, M., Salawitch, R., Harris, N., et al.: Chemical depletion of Arctic ozone in winter 1999/2000, J. Geophys. Res., 107, 8276, doi:10:1029/2001JD000533, 2002. 8292

Stohl, A., Eckhardt, S., Forster, C., James, P., Spichtinger, N., and Seibert, P.: A replacement of simple back trajectory calculations in the interpretation of atmospheric trace substance measurements, Atmos. Envir., 36, 4635–4648, 2002. 8292, 8302

Stohl, A., Cooper, O., and James, P.: A cautionary note on the use of meteorological analysis fields for quantifying atmospheric mixing, J. Atmos. Sci., 61, 1446–1453, 2004. 8303

Sutton, R., Maclean, H., Swinbank, R., O'Neill, A., and Taylor, F.: High-resolution stratospheric tracer fields estimated from satellite observations using Lagrangian trajectory calculations,

J. Atmos. Sci., 51, 2995–3005, 1994. 8287, 8289
Vanneste, J. and Haynes, P.: Intermittent mixing in strongly stratified fluids as a random walk, J. Fluid Mech., 411, 162–185, 2000. 8287
Waugh, D. and Plumb, R.: Contour advection with surgery: A technique for investigating fine scale structure in tracer transport, J. Atmos. Sci., 51, 530–540, 1994. 8290, 8303
Waugh, D., Plumb, R., Atkinson, R., Schoeberl, M., Lait, L., Newman, P., Lowenstein, M., Toohey, D., Avallone, L., Webster, C., and May, R.: Transport of material out of the stratospheric Arctic vortex by Rossby wave breaking, J. Geophys. Res., 99, 1071–1088, 1994. 8287, 8289
Waugh, D., Plumb, R., Elkins, J., Fahey, D., Boering, K., Dutton, G., Volk, C., Keim, E., Gao, R.-S., Daube, B., Wofsy, S., Lowenstein, M., Podolske, J., Chan, K., Proffitt, M., Kelly, K., Newman, P., and Lait, L.: Mixing of polar air into middle latitudes as revealed by tracer-tracer scatter plots, J. Geophys. Res., 102, 13 119–13 134, (96JD03715), 1997. 8288, 8295
Williamson, D. L.: Semi-Lagrangian moisture transport in the NMC spectral model, Tellus, 42A, 413–428, 1989. 8292
Woodman, R. and Rastogi, P.: Evaluation of effective eddy diffusive coefficients using radar observations of turbulence in the stratosphere, Geophys. Res. Lett., 11, 243–246, 1984. 8287

Table 1. Table of estimated Lagrangian diffusivity based on roughness curves for the 10 processed flights of the campaign and the return flights of 16 and 18 March. The two flights of 27 January 2000 and 11 March 2000 have been splitted into legs inside (i) and outside (o) the polar vortex.

Date	D from N_2O ($m^2\,s^{-1}$)	D from O_3 ($m^2\,s^{-1}$)
20 Jan.	$\gtrapprox 0.01$	$\gtrapprox 0.01$
27 Jan. i	$\gtrapprox 0.001$	$\gtrapprox 0.01$
27 Jan. o	$\gtrapprox 0.1$	$\gtrapprox 0.1$
31 Jan.	≈ 0.1	≈ 0.01
02 Feb.	$\lessapprox 0.1$	≈ 0.01
03 Feb.	≈ 0.01	$\gtrapprox 0.01$
26 Feb.	$\lessapprox 0.1$	$\gtrapprox 0.01$
05 March	≈ 0.1	≈ 0.01
07 March	≈ 0.1	≈ 0.01
11 March i	≈ 0.01	≈ 0.001
11 March o	≈ 0.01	≈ 0.05
12 March	≈ 0.1	$\lessapprox 0.1$
16 March	≈ 0.1	≈ 0.1
18 March	≈ 0.1	≈ 0.1

ACPD
4, 8285–8325, 2004

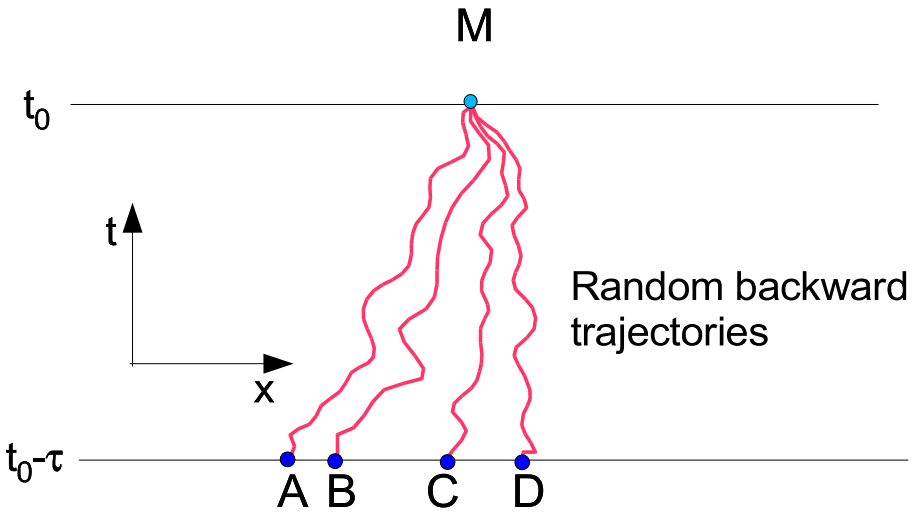

Fig. 1. Sketch of the trajectories of the transported and diffused particles meeting in point M at time t_0 after travelling from their initial locations (A, B, C, D) at time $t_0-\tau$. The mixing ratio in M and t_0 is reconstructed from averaging the mixing ratios in (A, B, C, D) and $t_0-\tau$.

ACPD
4, 8285–8325, 2004

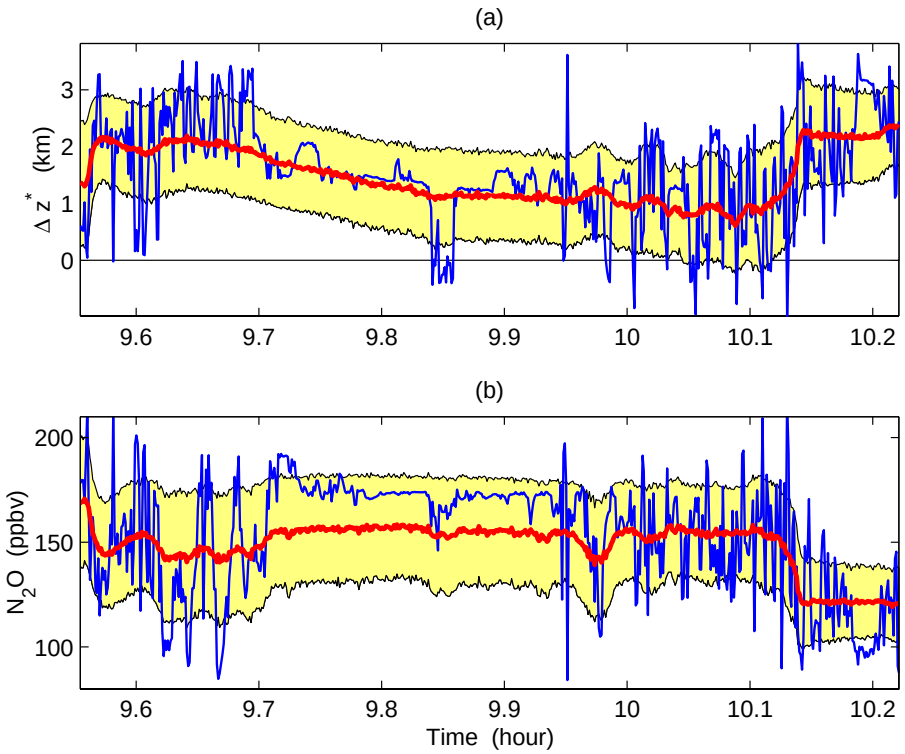

Fig. 2. **(a)** Vertical displacement Δz^* of the particles where $z^*=H_0 \ln(p/p_0)$ (p_0=1000 hPa, H_0=5850 m). In red: average displacement for the diffusive motion with D=0.01 m^2 s^{-1}; yellow area spans one standard deviation from the average; in blue: displacement for a single deterministic particle with no diffusion. Results are shown for backward integration over τ=38 days and one portion of the 27 January 2000 flight. **(b)** same as (a) but for the reconstructed N_2O mixing ratio.

ACPD
4, 8285–8325, 2004

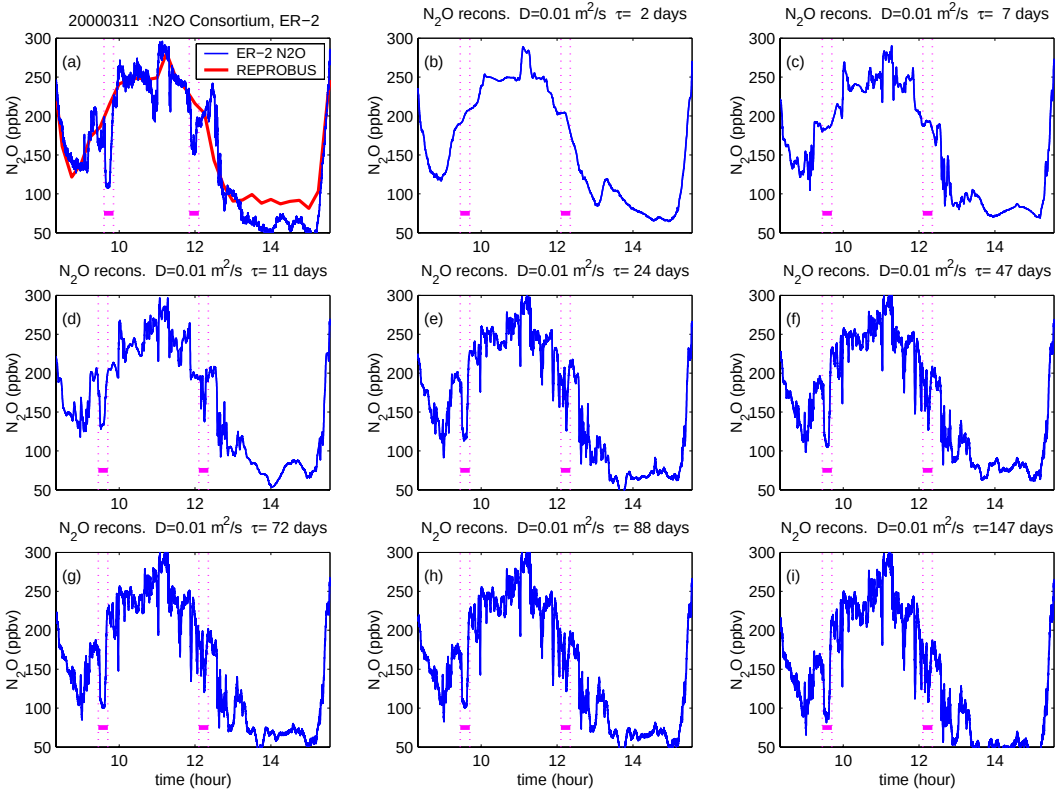

Fig. 3. Upper left panel: observed N_2O values and REPROBUS simulation for the 11 March 2000 flight. Other panels: sequence of reconstructed transects with D=0.001 $m^2\,s^{-1}$ and increasing value of τ up to 147 days. Marks and dotted lines indicate the location of the polar vortex sheet.

ACPD
4, 8285–8325, 2004

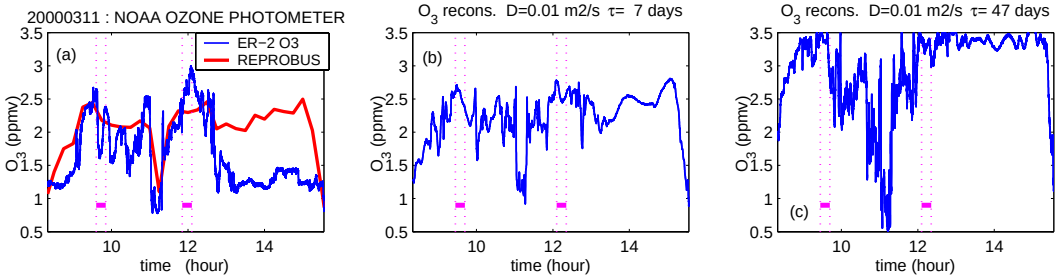

Fig. 4. Left panel: observed O_3 values and REPROBUS simulation for the 11 March 2000 flight. Central and right panels: reconstructed transects with D=0.01 $m^2\,s^{-1}$ and τ=7 and 147 days.

ACPD
4, 8285–8325, 2004

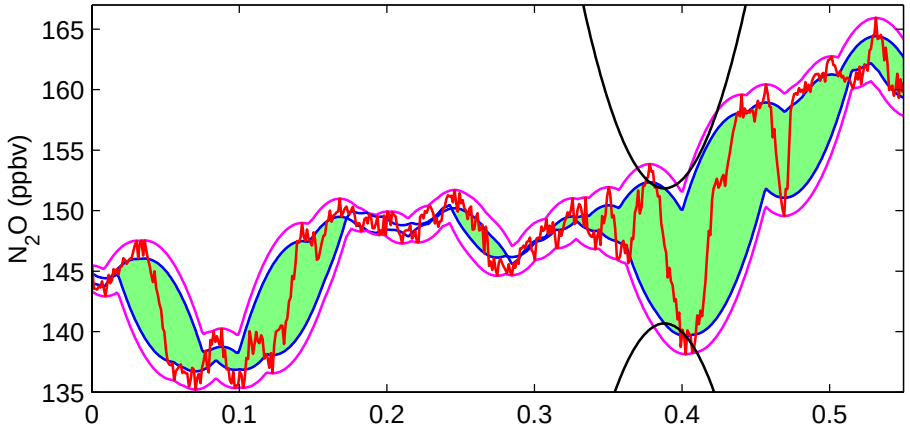

Fig. 5. The analysed curve (red) is bounded above and below by two osculating curves (magenta) tracing the tips of upper and lower osculating parabolas with parameter p. The positive area (green) between the two shifted osculating curves (blue) measures the roughness $\phi(p)$.

ACPD
4, 8285–8325, 2004

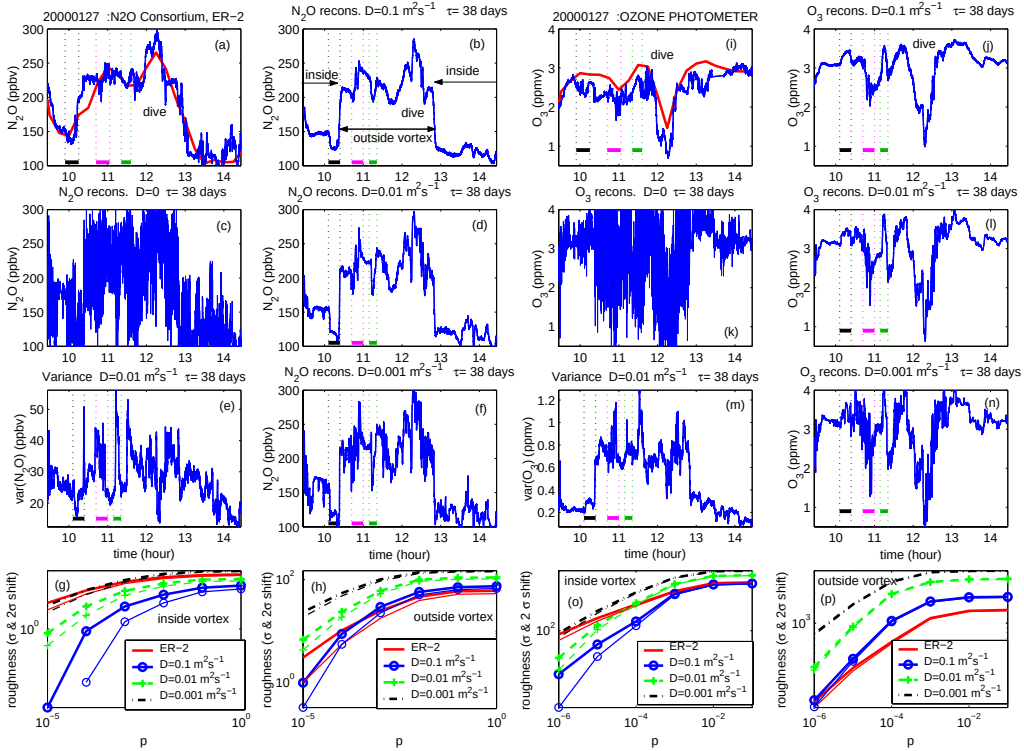

Fig. 6. Reconstructions and roughness for the 27 January 2000 flight. Left eight panels for N_2O and right eight panels for O_3. **(a)**: Observed (blue) and REPROBUS (red) N_2O. **(b, d, f)**: N_2O reconstructions for D=0.1, 0.01 and 0.001 $m^2\ s^{-1}$ at τ=38 days. **(c)**: Single deterministic trajectory N_2O reconstruction at τ=38 days. **(e)**: Variance of N_2O within the N particles released from each location. **(g)**: Roughness for observed and reconstructed transects as indicated in the legend, and for the flight segment located inside the polar vortex. Thick lines: shift is σ=3 ppbv; thin lines: shift is 2σ. **(h)**: Same as (g) but for the flight segment outside the polar vortex. **(i–p)**: Same as (a–h) but for O_3 and σ=10 ppbv. Three identified structures are marked in the figure. The peaks in N_2O and O_3 near 12 h are due to a dive of the ER-2 and are removed from roughness analysis.

ACPD
4, 8285–8325, 2004

Variability of the Lagrangian turbulent diffusivity in the lower stratosphere

B. Legras et al.

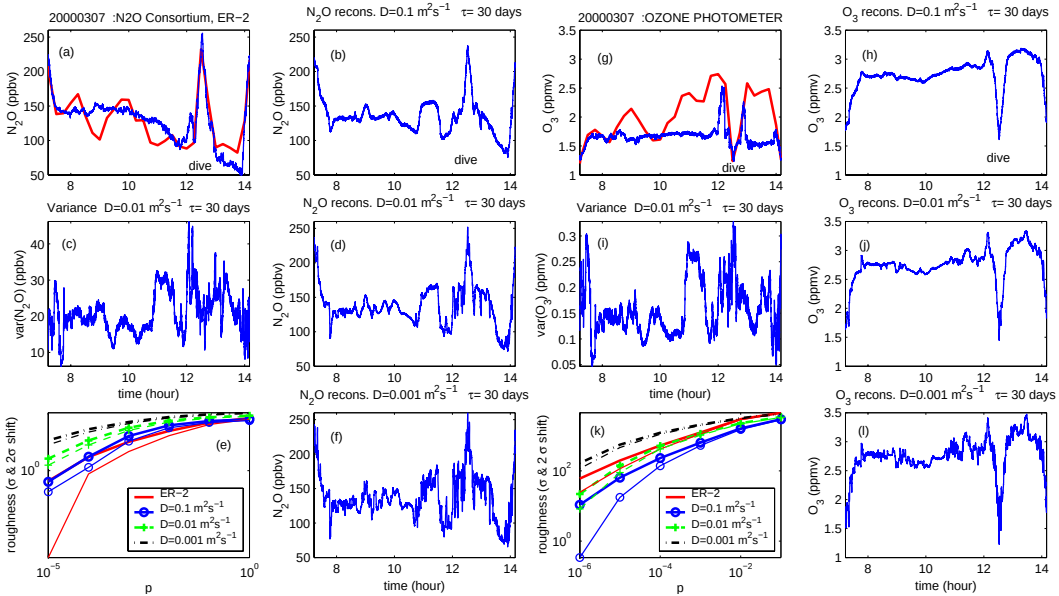

Fig. 7. Reconstructions and roughness for the 7 March 2000 flight inside the polar vortex. Left six panels for N_2O and right six panels for O_3. **(a)**: Observed (blue) and REPROBUS (red) N_2O. **(b, d, f)**: N_2O reconstructions for D=0.1, 0.01 and 0.001 $m^2\,s^{-1}$ at τ=34 days. **(c)**: Variance of N_2O within the N particles released from each location. **(e)**: Roughness for observed and reconstructed transects as indicated in the legend. Thick lines: shift is σ=3 ppbv; thin lines: shift is 2σ. **(g–l)**: Same as (a–h) but for O_3 and σ=10 ppbv.

ACPD
4, 8285–8325, 2004

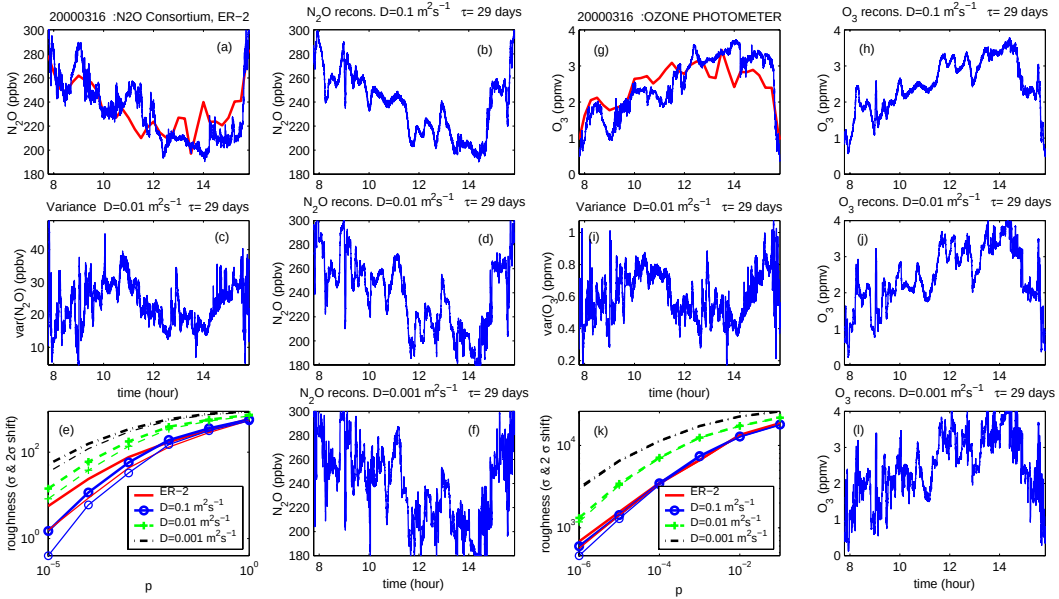

Fig. 8. Same as Fig. 7 but for the 16 March 2000 flight outside the polar vortex and τ=29 days.

ACPD
4, 8285–8325, 2004

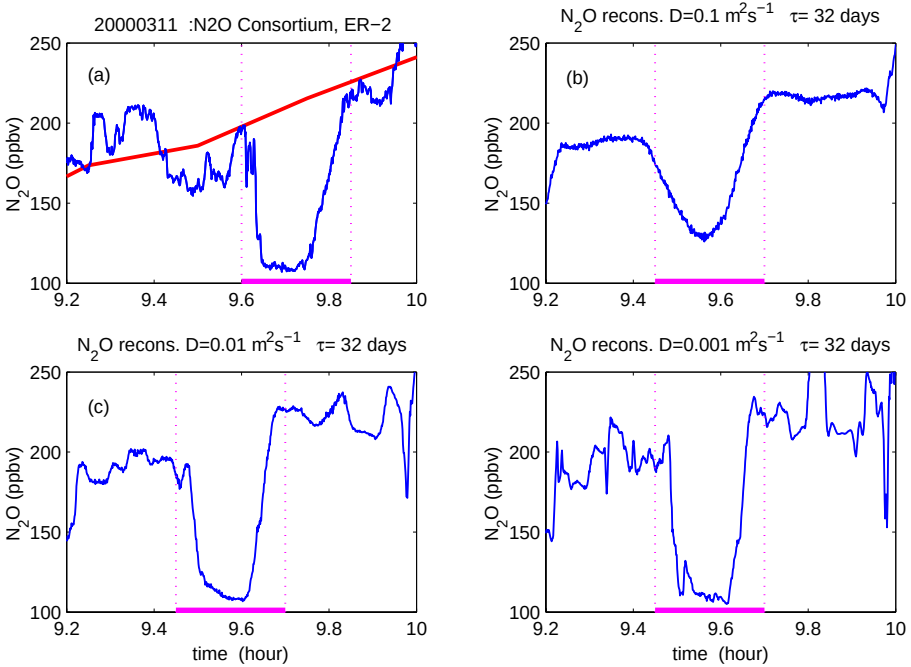

Fig. 9. Enlargement of observed and reconstructed transects encompassing the first crossing of the polar air sheet during 11 March 2000 flight. **(a)**: ER-2 (blue) and REPROBUS (red) N_2O. **(b–d)**: reconstructed N_2O for D=0.1, 0.01 and 0.001 $m^2\,s^{-1}$ for τ=32 days.

ACPD
4, 8285–8325, 2004

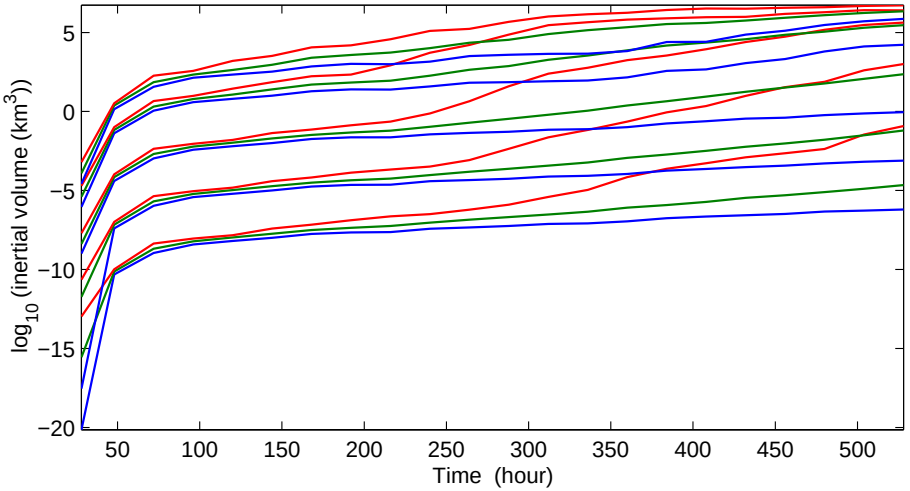

Fig. 10. Inertial volume calculated by fitting an ellipsoid to the cloud of N particles emitted from the flight track every 4 seconds. Families of curves from bottom to top: $D=10^{-8}\,m^2\,s^{-1}$, $D=10^{-6}\,m^2\,s^{-1}$, $D=10^{-4}\,m^2\,s^{-1}$, $D=10^{-2}\,m^2\,s^{-1}$, $D=10^{-1}\,m^2\,s^{-1}$. Green: average log(volume); blue: 5% percentile of the distribution; red: 95% of the distribution. The distribution consists in 500 points over a selected 2000 s section of the 27 January 2000 flight.

ACPD
4, 8285–8325, 2004

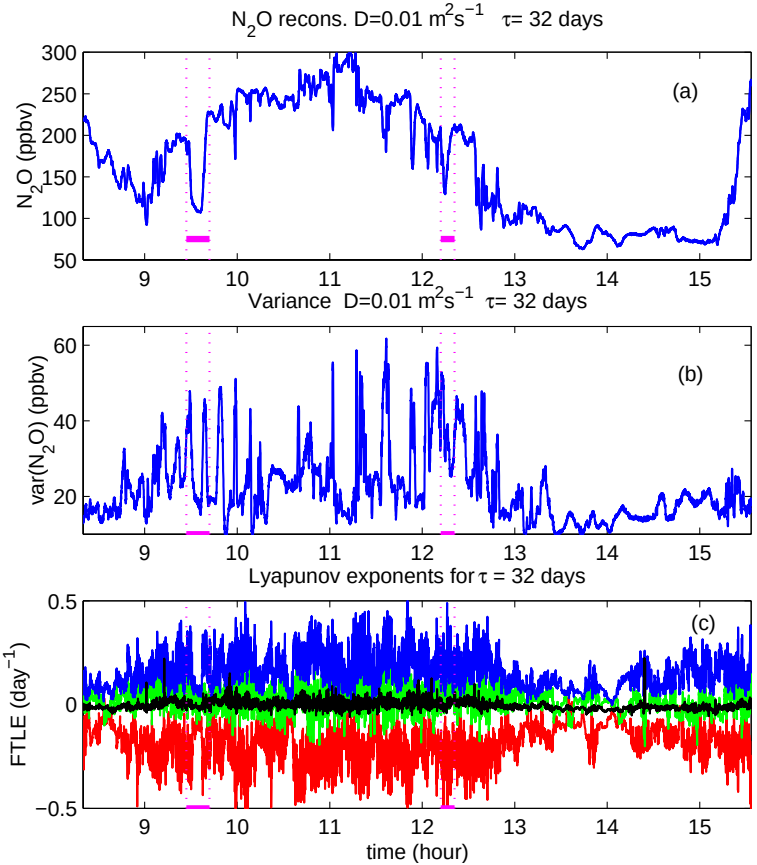

Fig. 11. **(a)** N_2O reconstruction for the 3 November 2000 flight with D=0.01 m^2 s^{-1} and τ=32 days. **(b)** N_2O variance of the N particles within each diffusive ensemble. **(c)** Lyapunov exponents, blue: λ_1, green: λ_2, red: λ_3, black: $\lambda_1 + \lambda_2 + \lambda_3$. The location of the polar air sheet crossings is marked.

ACPD
4, 8285–8325, 2004

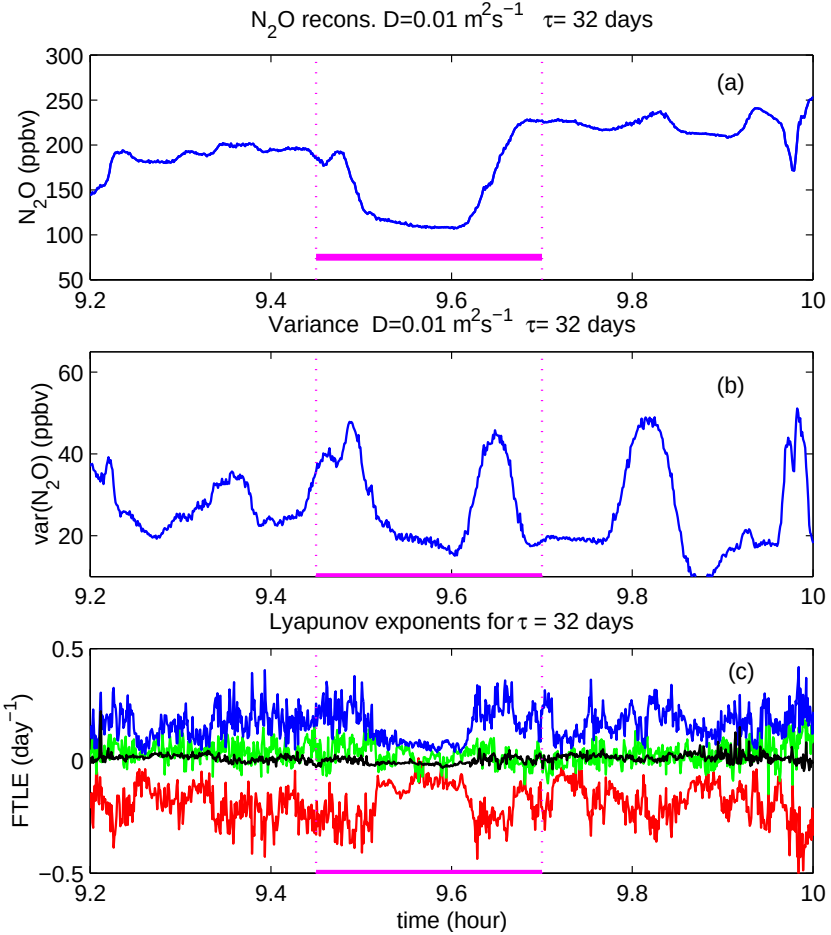

Fig. 12. Enlargement of Fig. 11 encompassing the first crossing of the polar air sheet.

ACPD
4, 8285–8325, 2004

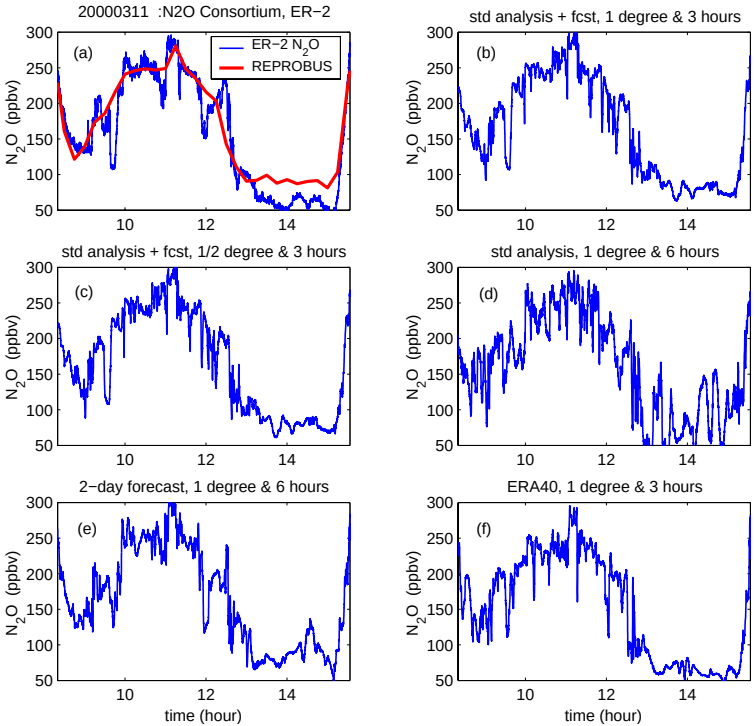

Fig. 13. Comparison of observed N_2O and reconstructions for different resolutions of the advecting wind. **(a)** Observed N_2O and REPROBUS prediction. **(b)**: Reconstructed N_2O using 3-hourly analysed and first guess winds on a 1° latitude-longitude grid which is the standard setting for all other figures. **(c)**: Same as (b) but for using a 0.5° grid. **(d)**: Same as (b) but for using only the 6-hourly analysed winds. **(e)**: Same as (d) but replacing the analysed winds by 6-hourly forecast winds generated twice-daily from the 48 and 54 h forecasts. **(f)**: Same as (b) but using the ERA-40 reanalysis instead of the operational analysis. All reconstructions are done with D=0.01 $m^2\,s^{-1}$ and τ=32 days.

ACPD
4, 8285–8325, 2004

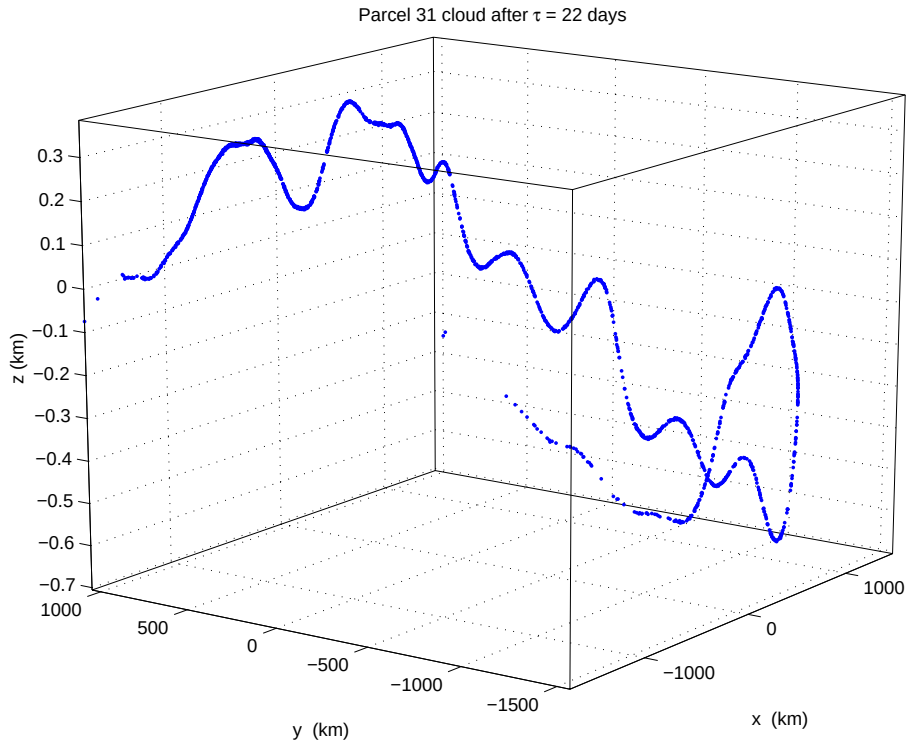

Fig. 14. Distribution of the cloud of points after τ=22 days for a parcel along the 11 March 2000 flight. Calculation done with D=10^{-4} m^2 s^{-1} in order to reduce lateral dispersion and to magnify the wavy pattern. It can be checked that dispersion occurs as a filament.

ACPD
4, 8285–8325, 2004